Anomalies in the low CMB multipoles and extended foregrounds

L. Raul Abramo*
Instituto de Física, Universidade de São Paulo
CP 66318, CEP 05315-970 São Paulo, Brazil

Laerte Sodré Jr.†
Departamento de Astronomia, Instituto Astronômico e Geofísico, Universidade de São Paulo
Rua do Matão, 1226 – 05508-090 São Paulo, Brazil

Carlos Alexandre Wuensche‡
Divisão de Astrofísica, Instituto Nacional de Pesquisas Espaciais
Av. dos Astronautas, 1.758, CEP 12227-010, São José dos Campos, Brazil
(Dated: May 11, 2006)

We discuss how an extended foreground of the cosmic microwave background (CMB) can account for the anomalies in the low multipoles of the CMB anisotropies. The distortion needed to account for the anomalies is consistent with a cold spot with the spatial geometry of the Local Supercluster (LSC) and a temperature quadrupole of order $\Delta T_2^2 \approx 50\,\mu K^2$. If this hypothetic foreground is subtracted from the CMB data, the amplitude of the quadrupole ($\ell = 2$) is substantially increased, and the statistically improbable alignment of the quadrupole with the octopole ($\ell = 3$) is substantially weakened, increasing dramatically the likelihood of the "cleaned" maps. By placing the foreground on random locations and then computing the likelihood of the cleaned maps we can estimate the most likely place for this foreground. Although the 1-year WMAP data clearly points the location of this hypothetical foreground to the LSC or its specular image (i.e., the vicinity of the poles of the cosmic dipole axis), the three-year data seems to point to these locations as well as the north ecliptic pole. We show that this is consistent with the symmetries of the cosmic quadrupole. We also discuss a possible mechanism that could have generated this foreground: the thermal Sunyaev-Zeldovich effect caused by hot electrons in the LSC. We argue that the temperature and density of the hot gas which are necessary to generate such an effect, though in the upper end of the expected range of values, are marginally consistent with present observations of the X-ray background of spectral distortions of the CMB.

PACS numbers: 98.80.-k, 98.65.Dx, 98.70.Vc, 98.80.Es

I. INTRODUCTION

The cosmic microwave background (CMB) anisotropies have been measured with very high accuracy by WMAP [1, 2]. Such a barrage of new data seldom brings only confirmation of known theories and mechanisms, and WMAP is no exception: lack of higher correlations [3] and some curious correlations between large-scale anisotropies are some of the most intriguing questions that have been raised by the WMAP data. In particular, two problems have been pointed with present CMB observations, using a wide variety of data, methods, maps and sky-cuts: first, that the quadrupole ($\ell = 2$) has a lower-than-expected signal [4, 5, 6]. Second, that the quadrupole and octopole ($\ell = 3$) present an unexpectedly high degree of alignment [4, 7, 8, 9, 10, 11, 12, 13]. The combined statistics of these effects implies that our CMB sky is only within the $\sim 0.01\%$ of randomly-generated maps with such anomalous quadrupole and octopole.

It is important to note, first, that these large-angle anomalies were already present in the COBE data [14], and they were confirmed by WMAP both in the 1-year and in the 3-year data releases [1, 2]. Second, even though the amplitude of the octopole C_3 has increased in the three-year compared to the first-year WMAP data, the statistical relevance of the deviant multipoles $\ell = 2$ and $\ell = 3$ has remained practically unchanged in the newly released three-year WMAP data [1], whereas the outliers of the first-year data [2] around $\ell \approx 20$, $\ell \approx 40$ and $\ell \approx 200$ have either disappeared or become much less of a source of concern in the 3-year data.

---

*Electronic address: abramo@fma.if.usp.br
†Electronic address: laerte@astro.iag.usp.br
‡Electronic address: alex@das.inpe.br

These large-angle anomalies have motivated many ingenious explanations, such as compact topologies [15, 16, 17], a broken or supressed spectrum at large scales [18] and oscillations superimposed on the primordial spectrum of density fluctuations [19]. When the low value of the quadrupole is combined with the alignment of the directions defined by these two multipoles (their "normal planes" – see [4, 7, 8, 9, 10, 11, 20]), the overall chance of such a statistical fluctuation is approximately 0.005% - 0.02% depending on the map and on the mask – i.e., only about one in 10000 randomly generated models have a lower C_2 *and* a more aligned quadrupole and octopole than the observed CMB sky.

As first noted by de Oliveira-Costa *et al.* [4], the directions preferred by the quadrupole and the octopole point roughly towards the Virgo cluster — which is in the general vicinity of the dipole and the equinox, and has been dubbed the "axis of evil" [9]. These large-scale anisotropies appear when one compares the northern/western galactic hemisphere (where Virgo and most of the Local Supercluster lie) with the southern/eastern hemisphere [3] as well. Unusually high correlations with the ecliptic have also been reported [8].

In this paper we investigate whether these large-scale anomalies can be due to extended (large-angle) foregrounds that have so far escaped detection. In particular, we re-examine a speculation by Abramo & Sodré [25] that the explanation for the observed properties of the quadrupole and octopole is a diffuse, large-angle CMB foreground spatially correlated with the region of the sky occupied by the local supercluster (LSC) – which is a spot roughly $50^o \times 30^o$ centered around Virgo, at $(l,b) = (284^o, 74^o)$. The peak temperature of this foreground would have to be of order $\sim 20\mu$K, with a root-mean-square average temperature of order $\sim 8\mu$K. Such a foreground would have the correct geometry to affect the quadrupole and octopole in a positive way, erasing their alignments and significantly increasing the amplitude of the quadrupole. One of the physical processes that could produce such a foreground is the thermal Sunyaev-Zeldovich effect (SZe) due to hot electrons in the intra-supercluster (ISC) medium [25]. For the range of frequencies observed by WMAP and COBE, the ISC gas causes an apparent decrease in the temperature of the CMB photons in the direction of the LSC. We have estimated, using a simplified model, that a temperature distortion as high as $|\Delta\hat{T}_{\ell=2}|_{rms} \approx 8~\mu$K is marginally consistent with present constraints on the ISC medium and with spectral distortions of the CMB.

The possibility that foregrounds could be responsible for the alignments was also noted in [26], and two recently related explanations were proposed by Rakic, Rasanen and Schwarz [27] and by Inoue and Silk [28]. Rakic *et* al. studied the Rees-Sciama effect due to a nearby large-scale structure (or structures), and found that the ensuing foreground could be as high as $\sim 30\mu$K, but that the phases were not right to eliminate the alignments and the low quadrupole.

Inoue and Silk, on the other hand, speculate that the non-gaussian cold spot in the southern galactic hemisphere [29] could be caused by voids in the nearby large-scale structure [28]. They conclude that the contribution from compensated pairs of voids would have the right phases to account for the low amplitude of the quadrupole and the for the unusual quadrupole-octopole alignment.

Notice that, because the quadrupole is even under parity transformations $\hat{n} \rightarrow -\hat{n}$, any given pattern has the same quadrupole components as its specular image. Since the effect discussed here relies mostly on a distortion of the quadrupole (which is both low-amplitude and has fewer phases than the octopole), this partly explains the apparent equivalence between the foreground proposed by Abramo & Sodré and foregrounds located in the southern galactic hemisphere, such as those proposed by Inoue & Silk. Furthermore, because most of the power of the observed CMB quadrupole lies in its $m=0$ and $m=\pm2$ components, another probable spot for an extended foreground corresponds to the location of Virgo, rotated 180° around the galactic poles axis – that is, $(l,b) \approx (100^o, 70^o)$.

By placing one of these hypothetical foregrounds (henceforth HFg) on random locations, removing it from a CMB map and then computing the likelihood of the "cleaned" map, we have been able to test the randomness of the spatial correlation with the four dual points described above. We find that, in all maps and in all foreground models tested, the most probable places for them are indeed either the vicinities of $\hat{n}_{LSC}$, $-\hat{n}_{LSC}$ or near the ecliptic poles.

We will show that, of all possible locations for this HFg, the LSC and its dual points produce the most significant improvements in the likelihoods of the CMB maps, by both increasing the (too low) level of the quadrupole C_2 and by weakening the (too high) quadrupole-octopole alignment. This can be achieved with HFg's whose rms temperatures lie in the range $5-15\mu$K and quadrupoles $C_2^{Fgrd} \sim 50-120\mu$K^2, depending on the model.

We have analysed the WMAP (1-year and 3-year) Internal Linear Combination maps [1, 2] (henceforth ILC), the map of Tegmark *et* al. [10, 21] (henceforth TOH), as well as the co-added maps based on 1-year and 3-year WMAP data (henceforth Coadded) For the ILC and Coadded maps we use the Kp2 maks, and for the TOH map we use the masks M0 and M6 described in [21]. In all cases the low value of the quadrupole and the alignments are robust, and removal of the HFg leads to dramatic increases in the likelihoods of the CMB maps. This strongly argues in favour of still unknown diffuse, large-angle structures around the dipole axis that may be affecting the CMB.

This paper is organized as follows: In Sec. II we summarize the multipole vector formalism and the statistics of alignments for CMB maps. In Sec. III we present a model of the HFg based on the LSC, and argue that it may be due to the Sunyaev-Zeldovich effect caused by hot gas in the intra-supercluster medium. In Sec. IV we consider the

spatial location of the foreground, and show that the association with the dipole axis is not an accident. We conclude in Sec. V.

II. LOW QUADRUPOLE AND ALIGNMENTS

Katz and Weeks [20] have described, in a beautiful paper, how to compute all multipole vectors given the spherical harmonic components $a_{\ell m}$ – see also [23]. The multipole vectors, introduced to CMB data analysis by Copi *et al.* [7], are essentially eigenvectors of a simple set of algebraic equation whose parameters are the multipole components. Very similar computations were conducted using other (usually numeric) methods in [3, 4, 8] to find these vectors. The idea, which goes back to J. C. Maxwell in the XIXth century, is that the multipole decomposition of a field on S^2 implies that for each moment ℓ there are ℓ eigenvectors of norm unity, $\hat{n}^{(\ell,p)}$. The bottom line of the multipole vector analysis is that the expansion in spherical harmonics is equivalent to an expansion in multipole vectors:

$$\frac{\Delta T_\ell(\theta,\varphi)}{T} = \sum_{m=-\ell}^{\ell} a_{\ell m} Y_{\ell m}(\theta,\varphi) = D_\ell \prod_{p=1}^{\ell} \hat{n}^{(\ell,p)} \cdot \hat{n}(\theta,\phi) - Z_{\ell-1}(\theta,\varphi) \,, \tag{1}$$

where $Z_{\ell-1}$ just subtracts the residual $\ell' < \ell$ total angular momentum parts of the product expansion, and is irrelevant to our analysis – see [20] for an enhanced discussion of the multipole vector expansion.

Notice that, contrary to the C_ℓ's, which are always positive-definite, the D_ℓ's can be either negative or positive. This means that the multipole vectors $\hat{n}^{(\ell,p)}$ define only directions [20], hence they are in fact "vectors without arrowheads". It can also be seen from the expansion above that, whenever using the multipole vectors to test for alignments, it is irrelevant what the amplitudes of the multipoles are – just their (complex) phases matter, of which there are ℓ for each multipole.

Starting with these ℓ multipole vectors one can also construct $\ell(\ell-1)/2$ normal vectors – or normal planes. Therefore, for $\ell = 2$ there are 2 multipole vectors ($\hat{n}^{(2,1)}$ and $\hat{n}^{(2,2)}$) and only one normal plane ($\vec{w}^{(2,1)} = \hat{n}^{(2,1)} \times \hat{n}^{(2,2)}$); for $\ell = 3$ there are 3 multipole vectors and 3 normal planes; and so forth. Notice that, because the multipole vectors are not necessarily orthogonal, the normal vectors need not be (and generally are not) of norm unity.

We can therefore check for "alignments" between either the multipole vector themselves, or between the normal planes. Two widely used tests that check for alignments of the quadrupole and octopole normal planes are the S statistic:

$$S \equiv \frac{1}{3}|\vec{w}^{(2,1)} \cdot \vec{w}^{(3,1)}| + |\vec{w}^{(2,1)} \cdot \vec{w}^{(3,2)}| + |\vec{w}^{(2,1)} \cdot \vec{w}^{(3,3)}| \,, \tag{2}$$

and the D statistic, which is analogous to S but disregards the norm of the normal vectors:

$$D \equiv \frac{1}{3}|\hat{w}^{(2,1)} \cdot \hat{w}^{(3,1)}| + |\hat{w}^{(2,1)} \cdot \hat{w}^{(3,2)}| + |\hat{w}^{(2,1)} \cdot \hat{w}^{(3,3)}| \,. \tag{3}$$

It can be easily seen that both S and D lie within the interval $(0,1)$. In what follows we will use mostly the S statistic, since the D statistic disregards the norm of the normal vector and therefore throws away some information about the system. For the higher multipoles this may not be much of an issue, but the quadrupole has only 2 complex phases (4 effective degrees of freedom) and we would like to retain as much of that phase information as possible.

One can easily compute the probability distribution functions (P.D.F.'s) for S and D using randomly-generated ("mock") maps, either by simulating maps, computing the harmonic components and then the vectors and alignments, or by directly simulating the harmonic components, which are Gaussian random numbers with dispersion given by $\langle|a_{\ell m}|^2\rangle = C_\ell$. Because the alignments do not depend on the C_ℓ's, but only on the phases between the $a_{\ell m}$'s, one need not adjust the level of the C_ℓ for each ℓ – all that is needed to test for the alignments in mock maps is the fact that the phases are random within each multipole.

In Fig. 1 we show the normalized P.D.F.'s for the S and D tests that were computed using 300.000 mock maps. As mentioned above, in what follows we will use mostly the S statistic, but we note that the D statistic gives similar results. For a complete treatment of statistical tests of isotropy, their P.D.F.'s, and an assessment of other sources of error see [24].

Statistics of large-angle anisotropies and the low quadrupole

Given a CMB map, the harmonic components can be easily extracted (we use HEALPix [30]), and the multipole vectors and their statistics can be easily computed. There are several maps to choose from, the most well-known
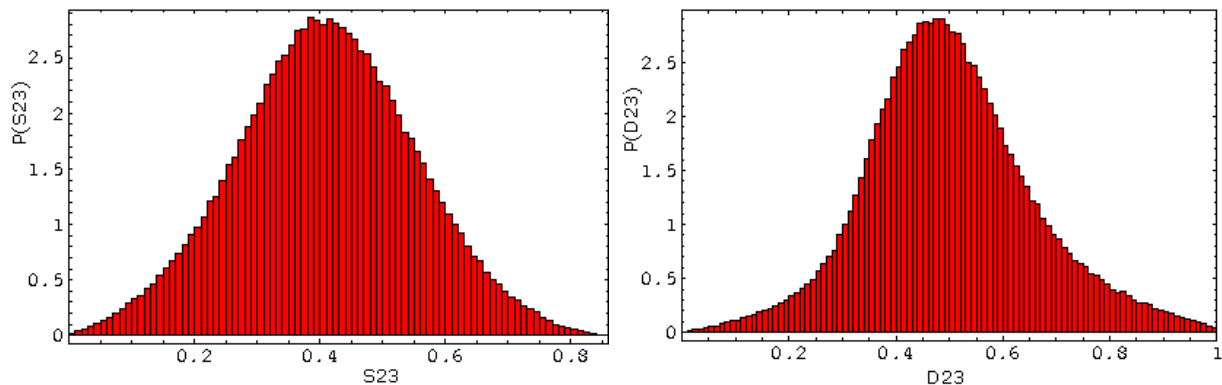
FIG. 1: Normalized P.D.F.'s for the S statistic (left panel) and D statistic (right panel), found by simulating 3×10^5 mock maps, binned in intervals of 0.01.

CMB Map	C_2 (μK^2)	$P_-(C_2)$	S	$P_+(S)$	P_{Tot}
TOH$_{\text{Mask 0}}$	201.2	3.43×10^{-2}	0.797	2.04×10^{-3}	1.6×10^{-3}
TOH$_{\text{Mask 0}}$ - LSC	340.6	1.02×10^{-1}	0.537	1.99×10^{-1}	2.5×10^{-1}
TOH$_{\text{Mask 6}}$	242.0	5.09×10^{-2}	0.776	4.04×10^{-3}	4.1×10^{-3}
TOH$_{\text{Mask 6}}$ - LSC	399.7	1.38×10^{-1}	0.531	2.19×10^{-1}	3.3×10^{-1}
Coadded (1yr)	97.7	6.69×10^{-3}	0.748	1.15×10^{-2}	1.2×10^{-3}
Coadded (1yr) - LSC	222.3	4.25×10^{-2}	0.509	2.85×10^{-1}	1.3×10^{-1}
Coadded (3yr)	100.5	7.16×10^{-3}	0.746	1.15×10^{-2}	1.3×10^{-3}
Coadded (3yr) - LSC	174.7	2.52×10^{-2}	0.590	1.17×10^{-1}	4.1×10^{-2}
ILC (1yr)	139.7	1.53×10^{-2}	0.727	1.74×10^{-2}	4.1×10^{-3}
ILC (1yr) - LSC	277.6	6.77×10^{-2}	0.537	2.19×10^{-1}	1.7×10^{-1}
ILC (3yr)	111.7	9.15×10^{-3}	0.720	2.10×10^{-2}	3.0×10^{-3}
ILC (3yr) - LSC	207.8	3.68×10^{-2}	0.538	2.19×10^{-1}	9.7×10^{-2}

TABLE I: Quadrupoles and alignments of CMB maps with and without the hypothetical LSC foreground subtracted. Shown are the Coadded and ILC maps with the 3-year KP2 mask [1, 2], and the TOH map with and without the mask described in [10] (based on first year WMAP data). $P_-(C_2)$ is the probability that a random map has quadrupole as low as C_2, and $P_+(S)$ is the probability that a random map has a quadrupole-octopole alignment as high as S. Also shown (last column) is the unbiased joint probability $P_{\text{Tot}} = 16 \times P_-(C_2) \times P_+(C_2) \times P_-(S) \times P_+(S)$, which estimates the likelihood that a random map has an anomalous (too high or too low) quadrupole *and* an anomalous (too high or too low) quadrupole-octopole alignment. In all cases, removal of the foreground leads to an improvement of about two orders of magnitude in P_{Tot}.

being the Coadded, ILC, LILC, TOH and the Q-, V- and W-band frequency maps. For all except the TOH map (which is already cleaned) we have use the KP2 mask based on three-year WMAP data [1].

It must be noted that the relativistic Doppler correction to the quadrupole is an important factor that must be subtracted from the maps, since it corresponds to a non-primary source of the quadrupole [8].

In Table I we present the quadrupoles and their alignments with the octopoles, for a few CMB maps. The Coadded and ILC maps use 3-year WMAP data, while the TOH map uses the first-year WMAP data only. The alignments are robust in all maps, as has been noted by [8, 9, 10]. In the next section we will construct a model foreground based on the LSC, and Table I presents the statistical effect of the subtraction of this LSC-shaped foreground. Notice that the relative error for the probabilities can be estimated as $\Delta P(X)/P(X) \sim 1/\sqrt{300.000 \times P(X)}$.

III. HYPOTHETICAL FOREGROUND

As first noted by de Oliveira-Costa *et al.* [4, 10], both the quadrupole and the octopole seem to be aligned on the plane defined by the direction $(l, b) \approx (250^o, 60^o)$, which is quite close to the Virgo cluster. This motivated the proposal of Abramo & Sodré [25], who speculated that the low-ℓ anomalies of the CMB could be explained by the Sunyaev-Zeldovich effect caused by hot electrons in the intra-supercluster medium of the LSC. For the frequency
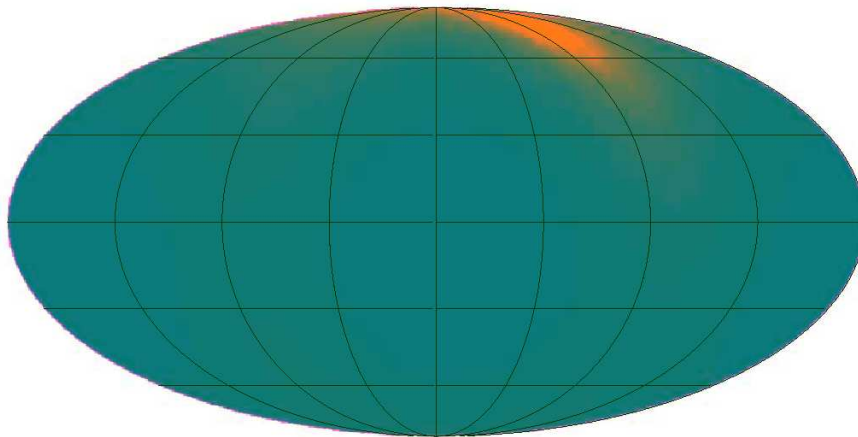
FIG. 2: Projected volume of the LSC on a Mollweide projection – the left edge corresponding to $l = 0^o$, the middle meridian to $l = 180^o$ and the horizontal line to $b = 0^o$ in galactic coordinates. Virgo is at the center of the LSC, at $(l, b) \approx (284^o, 74^o)$.

channels observed by COBE and WMAP, this effect would cause a cold spot with the shape and location of the supercluster superimposed on the primary CMB data.

We will show next that there are strong indications that an LSC-related foreground (or some structure diametrically opposite to the LSC) is distorting the observed CMB sky. Whether or not that foreground is caused by the SZe [25], a void [28], some other mechanism such as the Rees-Sciama (or Integrated Sachs-Wolfe) effect [27], or even a combination of those, remains to be seen.

A. Shape and location of the Local Supercluster

The morphology of the LSC is relatively well known [31]: it is a flattened collection of groups and clouds of galaxies centered at the Virgo Cluster, which contains ∼20% of its bright galaxies. The Local Group is dynamically linked to the LSC, and lies ∼15 Mpc from Virgo, at the border of the LSC. Notice that the LSC itself is not a virialized structure, hence the gas in its midst is not necessarily in equilibrium.

Since we are interested in an analytic approach at this point, a radical simplification will be made, approximating the shape of the LSC by an oblate spheroid of maximal radius 20 Mpc with approximate axial ratios 6:2:1 [31]. Therefore, our simple model assumes that the LSC is a collection of objects (clouds, groups and the Virgo cluster) which are distributed smoothly across the spheroid. The Sun stands at the margin of the spheroid (which looks like a flattened rugby ball), approximately 15 Mpc away from Virgo.

In our foreground model we assume that the intensity of the temperature decrement is proportional to the volume of the LSC, projected along the line of sight (i.e., the surface density.) This must be roughly correct, whatever the source of the hypothetical foreground, if it is indeed correlated with a diffuse structure such as the LSC. It is trivial to compute the surface density, given the shape and orientation of the LSC, and the result of this projection can be seen in Fig. 2 for an arbitrary (but constant) density. In that figure it can also be seen that our LSC model's projection on our sky is a spot of roughly $50^o \times 30^o$.

The oblate spheroid, in a conveniently rotated frame, is defined by the surface:

$$\left(bx' \right)^2 + \left(cy' \right)^2 + z'^2 = A^2 \ , \tag{4}$$

where A is the major axis (along the direction z'), and b and c are the ratios of the minor axes to the major axis.

The LSC parameters are $A \approx 20$ Mpc, $b \approx 3$ and $c \approx 6$. With these values the semi-major axes are $B = A/b \approx 6.7$ Mpc and $C = A/c \approx 3.3$ Mpc. Assuming that the Sun is located at a distance R under the z'-axis of the spheroid, the distance to the surface of the spheroid along lines-of-sight emanating from the Sun are given by:

$$
\begin{aligned}
r_S(\theta', \phi') \ = \ & \frac{1}{1 + \sin^2 \theta' \left[(b^2 - 1) \cos^2 \varphi' + (c^2 - 1) \sin^2 \varphi' \right]} \\
& \times \left[R \cos \theta' + \sqrt{ R^2 \cos^2 \theta' + (A^2 - R^2) \left[1 + \sin^2 \theta' \left((b^2 - 1) \cos^2 \varphi' + (c^2 - 1) \sin^2 \varphi' \right) \right] } \right] \ .
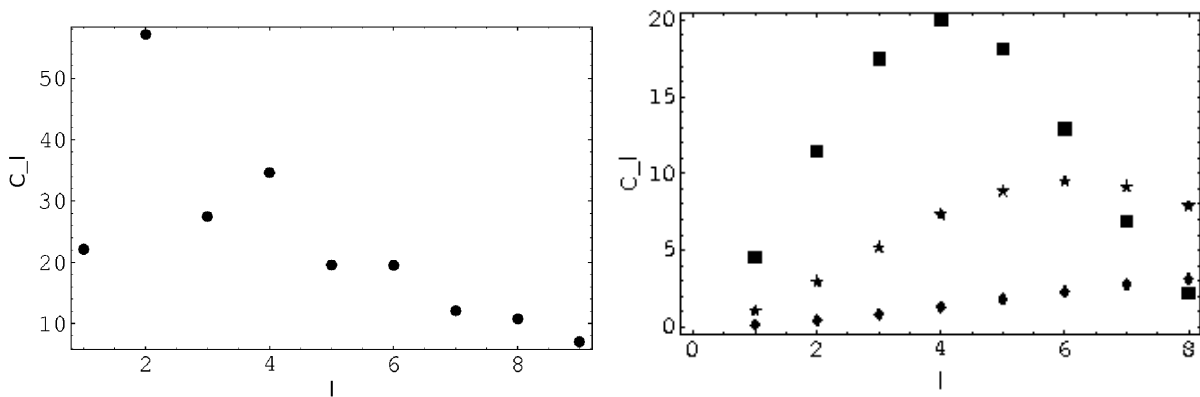\end{aligned} \tag{5}
$$

FIG. 3: Angular power spectra of the LSC foreground model (left panel), where we use $\alpha = 1$ – see Eq. (11); and of the Disk (uniform-temperature) foreground model, with angular diameters of 30° (diamonds), 50° (stars) and 70° (squares.)

Obviously, if the density is uniform inside the spheroid then the surface density will be proportional to r_S.

We can use the surface density of the LSC as the blueprint for a foreground, and therefore consider the temperature decrement caused by the foreground to be proportional to r_S. In Fig. 3 (left panel) we show the spectrum of anisotropies for such a model, where the proportionality constant is set by assuming that the effect is caused by scattering of the CMB photons by hot electrons in the ISC medium – see below. Notice that the quadrupole is substantially higher than the other multipoles, because the foreground's temperature is not constant as the line of sight moves away from the center of the LSC. This sorts out the quadrupole as the biggest contribution to the power spectrum, and in fact the RMS temperature fluctuation over the whole sky is well approximated by the quadrupole.

Given our ignorance about the existence, shape and form of this hypothetical foreground, we could equally well assume, following Inoue & Silk [28], that the temperature of the foreground is approximately uniform, falling quickly to zero away from the center of the spot. In Fig. 3 (right panel) we show the anisotropy spectra of three such spots – with angular diameters of 30°, 50° and 70°. The fact that the temperature is uniform inside the spot means that the low multipoles contribute more evenly to the foreground. Hence, for a given RMS temperature fluctuation there is less power in the quadrupole in the uniform-temperature foreground relative to the varying-temperature foreground. Moreover, as higher multipoles are more important in the uniform-temperature foreground, if that is the case then it may be possible to find independent corroborating evidence by searching for anomalous alignments in the higher multipoles (e.g., $\ell = 4$ and $\ell = 5$) as well. This will be analysed in Sec. IV.

B. Foreground model: Sunyaev-Zeldovich effect in the LSC

The SZe is caused by the inverse Compton scattering of CMB photons by hot electrons in the intra-cluster medium [32]. It is a nonthermal, frequency-dependent effect: the upscattering causes an incident blackbody spectrum of photons to become distorted in such a way that the resulting higher abundance of high-energy photons is compensated by a shortage of low-energy photons. The spectral distortion is given by [32]:

$$\frac{\Delta T(\theta, \varphi; \nu)}{T_0} = y(\theta, \varphi) \left(x \cotanh \frac{x}{2} - 4 \right) , \qquad (6)$$

where $T_0 = 2.726$K is the temperature of the CMB, y is the comptonization parameter in the direction $\hat{n}(\theta, \varphi)$ and $x = h\nu/k_B T_0$.

The frequency at which photons are neither depleted nor overproduced is $\nu_0 = 218$ GHz [33] — COBE/DMR and WMAP work in the range 20-90 GHz. For frequencies below ν_0 the effect is a nearly uniform reduction in the temperature of the photons, $\Delta T/T \approx -2y$, and for frequencies above that the effect is the opposite. This means that measurements over a range of frequencies around ν_0 (such as PLANCK's LFI and HFI [53]) can pick up the signal of the SZe and distinguish it from the primary anisotropies.

The comptonization parameter y measures an optical depth for the CMB photons created by the hot electrons, and its value is given by the product of the Thomson cross-section $\sigma_T = 6.65 \times 10^{-25}$ cm^2 times the temperature-averaged

density of photons along the line of sight [33]:

$$y = \int \sigma_T \frac{kT_e}{m_e c^2} n_e dl \ , \tag{7}$$

where T_e is the electron temperature, m_e is the electron mass and $dl = dl(\theta, \phi)$ is the line-of-sight distance element along the direction (θ, ϕ).

The SZe has been observed over the past few years in many clusters, but its weak strength means that it could only be detected in the central parts of clusters, where column densities of hot gas are sufficiently high [33, 34]. It is evident that some amount of SZ will take place also in the LSC, but the question is, how much? The answer depends on the gas density in the ISC medium, its temperature distribution, the morphology of the LSC and our position inside it.

Although the morphology of the LSC as traced by galaxies is well known, the density and temperature distribution of the gas of the ISC medium are not. Unfortunately, X-ray and microwave observations have not yet reached the level of sensitivity required to detect directly the very smooth, diffuse columns of hot gas in the outer regions of clusters. It seems, however, obvious that there must be a great amount of ionized gas in the ISC medium, among other reasons because the absence of observations of the Gunn-Peterson effect indicates that most of the ISC hydrogen must be ionized. The gas is thought to have been shock-heated at the time of galaxy formation, and now it is probably distributed in many phases, including filaments and a more homogeneous component [35, 36, 37]. Phillips, Ostriker and Cen [38] have constrained the amount of gas in filaments using numerical simulations and the X-ray background, and argued that this "warm-hot" ($kT \approx 100$ eV – 10 keV) gas can account for only 5–15 % of the "missing baryons". More recently, Nicastro *et al.* showed that this fraction could be as high as 27% [39]. It is therefore quite possible that much of this gas is in the ISC medium. So, the questions now are: how hot is this ionized gas, and how is it distributed?

Hogan was the first to propose that superclusters (and the LSC) could impact the CMB anisotropies through the thermal and kinetic Sunyaev-Zeldovich effects [40]. Molnar and Birkinshaw used HEAO 1 A2 [41] and COBE DMR data to analyze the Shapley supercluster and found no evidence of hot ($> 10^7$K) gas in the ISC medium [42]. Boughn [43], on the other hand, used the HEAO 1 A2 X-ray map and a simple "pillbox" model of nearly constant electron density in the LSC to argue that the SZe could be as high as $|\delta T| \sim (17 \pm 5)$ μK — although he assumed a gas temperature in the high end of the range 10^5–10^8 K. Kneissl *et al.* [44] did study the correlation of COBE DMR and ROSAT X-ray data away from the galactic plane, but it is not clear that the X-ray data has enough sensitivity to detect the diffuse hot gas of the LSC, and, in any case, the authors analyzed a region which misses a large chunk of the LSC.

Much work has been done to study the impact of the SZe from *distant* clusters on the CMB (see, e.g. [45, 46, 47, 48]). It has been found that the largest contribution to the angular power spectrum from the SZe comes from the most massive clusters ($M \sim 10^{15}h^{-1}M_\odot$), at scales $\ell \sim 3000$, with amplitudes $\ell(\ell+1)C_\ell/2\pi \approx 10 - 100\,\mu$K^2.

The overall number of free electrons in the LSC can be estimated given its gas fraction and mass:

$$N_e = \frac{M_{LSC}f_g}{\mu_e m_p} \ , \tag{8}$$

where M_{LSC} is the LSC mass, f_g is the gas fraction, μ_e is the molecular weight per electron and m_p is the proton mass. We may assume that the mass of the LSC is $\sim 7 \times 10^{15}$ M$_\odot$ [49]. Assuming that the Hydrogen is fully ionized and that the helium mass fraction is $Y = 0.24$, then $\mu_e = 1/(1 - Y/2) \simeq 1.14$.

The gas fraction is not very well known, but X-ray observations of clusters indicate that $f_g \approx 0.06h^{-3/2}$ [52]. The fraction could be different in the ISC medium, but we will assume for simplicity that the fraction in clusters is the same as outside. Using $h = 0.7$ we get finally that the total number of electrons in the LSC should be of order $N_e \sim 7 \times 10^{71}$.

A very simple model for the LSC gas is to neglect the gas phases and the substructures inside the supercluster, and to assume that the gas is uniformly distributed inside the LSC. Hence the total volume occupied by the gas is $V_{LSC} = 4\pi/3 \times ABC$ and therefore the average density of electrons in the LSC is approximately:

$$n_e = \frac{N_e}{V_{LSC}} \sim 1.3 \times 10^{-5} \text{cm}^{-3} \ . \tag{9}$$

On the other hand, the X-ray background is also an important constraint on the density and temperature of the ISC medium. A compilation of observations [20] gives a background flux for energies $h\nu \sim 2$ keV of approximately 10^{-25} erg s^{-1} cm^{-2} sr^{-1} Hz^{-1} over the whole sky. The expected flux at this energy due to thermal bremsstrahlung emission from LSC gas is $\sim 5 \times 10^{-26}$ erg s^{-1} cm^{-2} sr^{-1} Hz^{-1}. Since the X-ray flux is proportional to the square

of the electron density, if the gas temperature is indeed 2 keV, then the upper bound for the electronic density is of order $n_e \approx 5 \times 10^{-5}$ cm^{-3}. This corresponds to a collapse factor of only a few.

We can estimate the comptonization parameter assuming a constant electron density across the LSC. If the gas has an *average* temperature of 2 keV then $\langle kT_e \rangle / m_e c^2 \simeq 0.004$, and with a maximum line-of-sight distance (in the direction of Virgo) of ~ 30 Mpc we obtain that the comptonization parameter is at most:

$$\Delta y \approx \sigma_T \langle \frac{kT_e}{m_e c^2} \rangle \times n_e \times 30 \text{Mpc} \sim \frac{n_e}{5. \, 10^{-5} \text{cm}^{-3}} \times 10^{-5} \ . \tag{10}$$

The comptonization parameter can be exactly computed from Eq. (7) for our oblate spheroid model, if we assume that the density and temperature of the hot gas is uniform inside the LSC, and zero outside it. In that case the comptonization parameter is proportional to the projected distance to the surface of the spheroid, Eq. (5). The resulting angular power spectrum for the SZe of the LSC in this model is given in Fig. 3. The amplitude of the SZe quadrupole is:

$$\Delta \hat{T}_2^2 \ \equiv \ \frac{6}{2\pi} \hat{C}_2 \approx 60 \, \alpha^2 \, \mu\text{K}^2 \ , \tag{11}$$
$$\alpha \ = \ \frac{n_e}{5 \times 10^{-5} \text{cm}^{-3}} \times \frac{\langle kT_e \rangle}{2 \, \text{keV}} \ .$$

This level of temperature distortion is consistent with the COBE FIRAS limit on deviations from the blackbody spectrum on large angular scales [50].

Recently, Dolag et al. [51] have studied the imprint of the local superclusters on the CMB via the SZe. They have used constrained simulations to study these local structures, and their conclusion was that the thermal SZe is too small, by at least one order of magnitude, to affect either the quadrupole or the octopole. It is clear that the SZe model presented here cannot account for the anomalous quadrupole and octopole if the density and temperature of the gas in the ISC medium lie near the conventionally accepted limits, which are derived in part from observations and in part from simulations such as those done by Dolag et al., which include baryons, gas flows and feedback mechanisms. Therefore, if our model is correct, then either the mechanisms that endow the ISC medium with gas are still not entirely understood, or the global parameters and initial conditions have to be changed (which is less likely.) Another possibility is that the SZe is not the only source of foreground, in which case a combination of foregrounds (all spatially correlated so the effects add up) is responsible for the distortions. In fact, such a combination of effects is not unlikely, since all local structures are composed of multi-phase gas and other foreground sources.

IV. GEOMETRY AND LOCATION OF THE FOREGROUND

In Table I we showed the effect of subtracting the HFg based on the projected volume of the LSC. This HFg peaks at the center of the LSC and falls steadily as the line of sight moves from the center of the LSC. When the HFg is subtracted from a full CMB sky, both the quadrupole is enhanced and the quadrupole-octopole alignment is weakened. This means that, whatever the source of the HFg in the LSC (or its specular image), the geometry of the LSC is such that the foreground's phases for the quadrupole and octopole work in the direction of correcting for the low quadrupole and for the high quadrupole-octopole alignment of the CMB maps.

We can test the spatial location, shape and orientation of this HFg, and check whether these are indeed correlated with the properties of the LSC, or if the improvement in the quadrupole level and in the alignments are just flukes that could have happened whatever the location of the HFg. This can be done by rotating the foreground maps by arbitrary Euler angles, and then computing the effect of subtracting them from the CMB maps.

We employ an unbiased measure of the likelihood of the maps defined by:

$$P_{Tot} = 2^4 P_+(C_2) P_-(C_2) P_+(S) P_-(S) = 2^4 P_+(C_2)[1 - P_+(C_2)] P_+(S)[1 - P_+(S)] \ . \tag{12}$$

This estimator is maximal ($P_{Tot} = 1$) for a map whose quadrupole C_2 and alignment S are equal to their respective expectation values – in which case $P_-(\bar{C}_2) = P_+(\bar{C}_2) = P_-(\bar{S}) = P_+(\bar{S}) = 1/2$.

We will consider two HFg models: the LSC model described by Eq. (5) (hereafter HFg-LSC), and a model inspired by the proposal by Inoue & Silk [28] – a nearly homogeneous disk with a diameter of 50° (hereafter HFg-D.) It should be noticed that the HFg-D model must have a higher temperature distortion in order to cause the same order-of-magnitude effect in the likelihoods, compared to the HFg-LSC model. The reason is simple, and can be inferred from Fig. 4: since the HFg-D model has nearly homogeneous temperature, all low multipoles have similar amplitudes. The temperature in the HFg-LSC model, on the other hand, falls steadily from the center of the LSC, and this
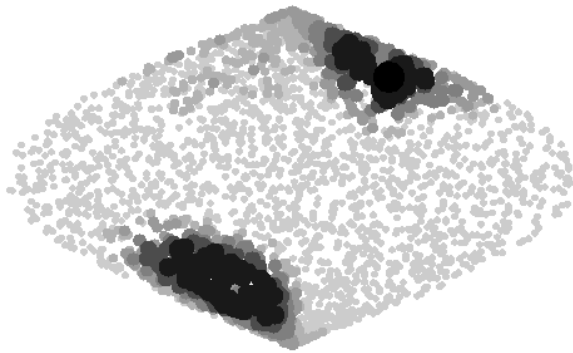
FIG. 4: Locations of the HFg-LSC model applied to the "mask 0" TOH map [10, 21]. The largest, darkest spot marks the top foreground as measured by the highest values of P_{Tot} obtained after 3000 random rotations of the putative foreground. The top 5%, 10%, 15% and 33% foregrounds are indicated by the progressively smaller and lighter spots. The smallest, lightest spots mark the bottom 67% locations. Here and in Figs. 6-16, instead of the Mollweide projection, we use a simple map $(\theta, \varphi) \rightarrow (\theta, \varphi \sin \theta)$.
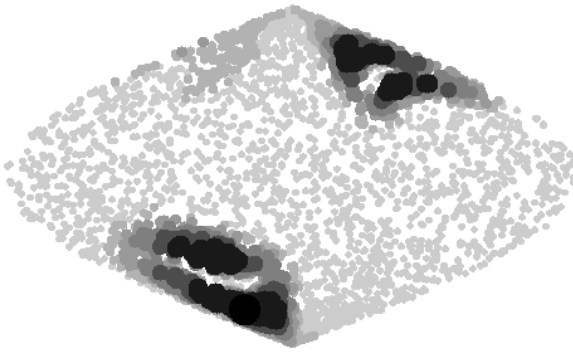
FIG. 5: Same as before, in the case of the HFG-D model applied to the "mask 0" TOH map [10, 21].

angle dependence coincides roughly with the angular dependence of the quadrupole. Therefore, the amplitude of the temperature distortion in the HFg-D model must be higher than in the HFg-LSC model in order to get the same level of the quadrupole. So, whereas in the HFg-LSC model the peak temperature distortion is of order -90μK, with a quadrupole $C_2 \approx 60\mu\text{K}^2$, for the HFg-D model to get the same quadrupole the temperature of the $50^o \times 50^o$ spot must be $T_{Disk} \approx -130\mu$K.

For each model we rotate the putative foreground by random Euler angles and subtract it from a CMB map to obtain the "cleaned" map. We then look for the corrected maps with highest likelihoods, as measured by the largest value of the unbiased probability P_{Tot}. We used 2000 random rotations for each foreground model and for each map of Table I (all with the KP2 mask applied.)

The results are shown in Figs. 5-16, where each spot marks the location of a hypothetical foreground. The dark spots mark the locations of the top 5% of foregrounds as measured by the likelihood of the cleaned maps. The lighter, smaller spots mark the location of the top 10%, 20% and so forth. The bottom 50% locations are shown as the smallest, lightest spots. The top foreground in each case is shown in Table II, along with its location and likelihood.

It can be seen from Figs. 5-16 that, in most cases, there is a strong clustering of the preferred locations around Virgo (and the LSC), its diametrically opposite point, and the region which correspons to Virgo rotated 180° around the z-axis. The preferred locations seem to be more scattered for the 3-year Coadded map with both foreground models, and for the ILC maps with the HFg-LSC model.

There is a simple explanation for the spatial distribution seen throughout Figs. 5-16: the HFg's change P_{Tot} mostly by amplifying and rotating the quadrupole of the original maps. But the quadrupole is even under parity transformations $\hat{n} \rightarrow -\hat{n}$, therefore from the point of view of the quadrupole, it is irrelevant if the foreground is at the LSC or at its diametrically opposite side. Moreover, since most of the power of the quadrupole lies in its $\ell = 2, m = 0$ and $\ell = 2, m = \pm 2$ components, a rotation by 180° degrees effects very little change to it. Therefore, if the foreground which is distorting the CMB is indeed at the LSC, then its preferred locations in a blind search will degenerate to
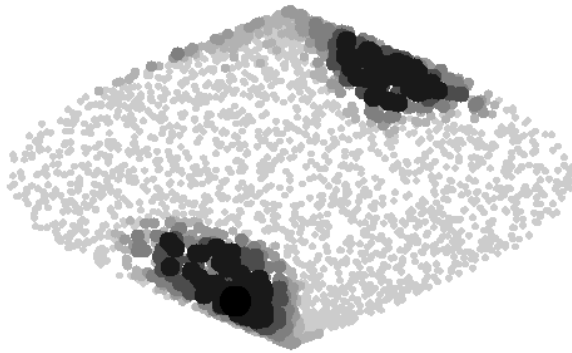
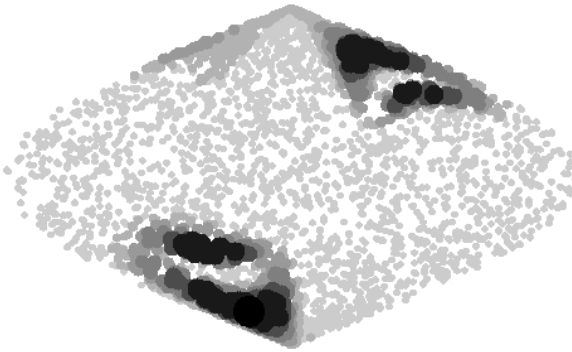FIG. 6: Same as before, in the case of the HFg-LSC model applied to the "mask 6" TOH map [10, 21].

FIG. 7: Same as before, in the case of the HFg-D model applied to the "mask 6" TOH map [10, 21].

not only the vicinity of the LSC itself, at $(l, b) = (284^o, 74^o)$, but also to its "dual points" at $(l, b) \approx (104^o, -74^o)$ and $(l, b) \approx (104^o, 74^o)$. This is indeed what seems to happen for most maps – see Table 2.

It is interesting to notice that, even though the amplitude of the octopole of the HFg-LSC model is subdominant, in the HFg-D model there is a substantial change in the octupole after the subtraction. Although the impact of the octopole in P_{Tot} is small, there are other statistical tests which are sensitive to it – in particular, the $S^{(4,4)}$ statistic of Copi *et al.* [7, 8] which tests for an alignment of the quadrupole and octopole with the ecliptic plane. The 3-year Coadded and ILC maps have too high values of $S^{(4,4)}$ at 99.5% C.L. After subtracting the best-fit Disk foreground model, those values come down to 84% C.L. for the Coadded map and to 98% C.L. for the ILC map.
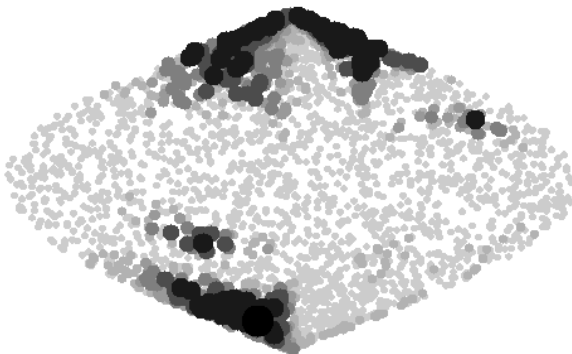

FIG. 8: Same as before, in the case of the HFg-LSC model applied to the 1-year Coadded map.
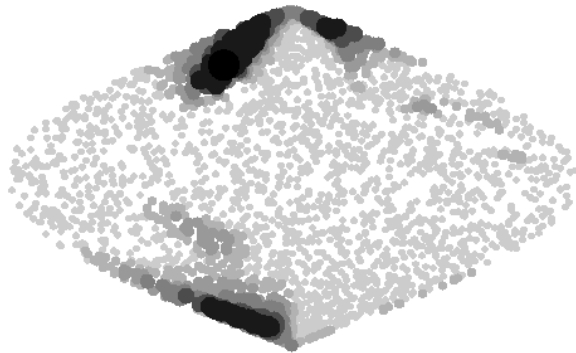
FIG. 9: Same as before, in the case of the HFg-D model applied to the 1-year Coadded map.
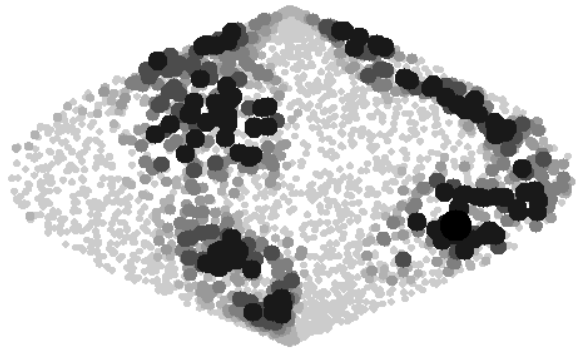

FIG. 10: Same as before, in the case of the HFg-LSC model applied to the 3-year Coadded map.

A. Higher multipoles

If the HFg indeed exists, it may be possible to detect correlations in the higher ℓ components as well. However, depending on the model, the spectrum of the foreground can decay with large ℓ, and the increasing number of phases means that these correlations will probably difficult to detect. If the foreground is homogeneous (as in the Disk model), the higher multipoles can also become important and their presence may affect the alignments between, say, $\ell = 2 - 5$.

It is trivial to generalize the tests of Eqs. (2)-(3) for higher multipoles – see, e.g., [20, 24]. If a given foreground cures the quadrupole level and the quadrupole-octopole alignment at the cost of introducing anomalous alignments between other multipoles, then the overall likelihood of the resulting map should fall. On the other hand, if the
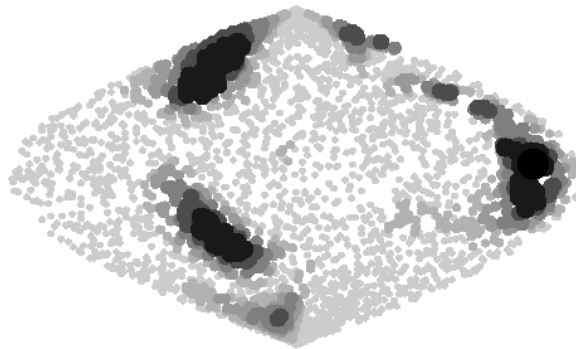

FIG. 11: Same as before, in the case of the HFg-D model applied to the 3-year Coadded map.
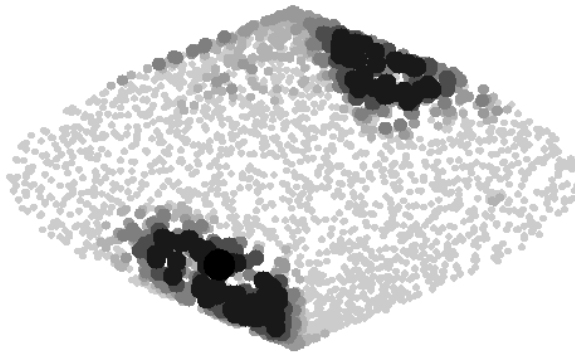
FIG. 12: Same as before, in the case of the HFg-LSC model applied to the 1-year ILC map.
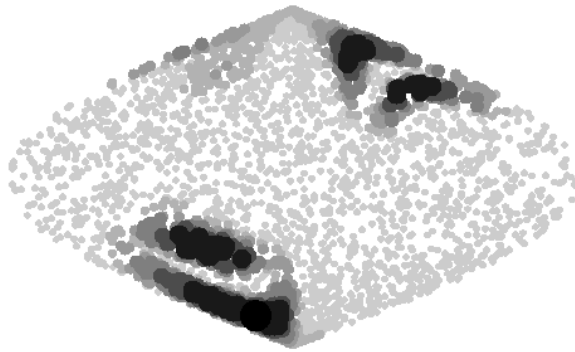

FIG. 13: Same as before, in the case of the HFg-D model applied to the 1-year ILC map.

original CMB map has another anomalous alignment which is relaxed because of the hypothetical foreground, then the likelihood of the resulting map increases even further.

We have tested the maps of Table II for signs of anomalous alignments between the higher multipoles using an unbiased probability with 38 tests, P_{38} – which includes the level of the quadrupole and the quadrupole-octopole alignment [24]. The results are mixed, and probably reveal intrinsic differences between the maps, masks and foreground models. For example, whereas the original TOH map with the Mask 6 [10, 21] has $P_{38} = 3.5 \times 10^{-15}$, subtraction of the best-fit HFg-LSC model leads to an improvement to $P_{38} = 3,5 \times 10^{-10}$, while subtraction of the best-fit HFg-D model improves it to $P_{38} = 2,4 \times 10^{-7}$. For the Coadded map (3-year data) with the KP2 mask [1, 2], the original map has $P_{38} = 4.4 \times 10^{-13}$, and after subtracting the best-fit HFg-LSC model it only improves to $P_{38} = 1,1 \times 10^{-9}$, while subtraction of the best-fit HFg-D model leads to $P_{38} = 3,7 \times 10^{-8}$. Notice that in all cases above, the level of
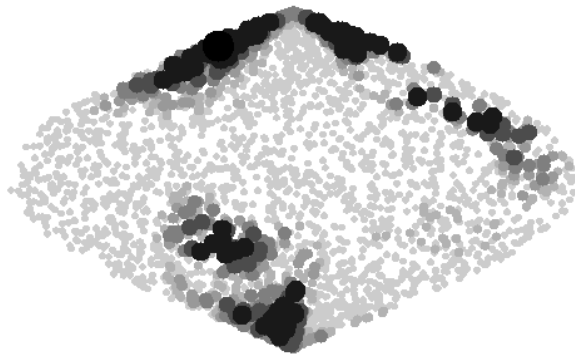

FIG. 14: Same as before, in the case of the HFg-LSC model applied to the 3-year ILC map.
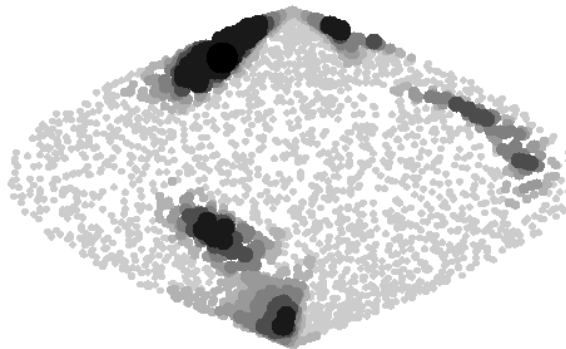
FIG. 15: Same as before, in the case of the HFg-D model applied to the 3-year ILC map.

CMB Map - Foreground	P_{tot}	(l, b)
$TOH_{Mask\ 0}$ - LSC	0.380	(136,-51)
$TOH_{Mask\ 0}$ - Disk	0.231	(152,-69)
$TOH_{Mask\ 6}$ - LSC	0.488	(156,-63)
$TOH_{Mask\ 6}$ - Disk	0.363	(159,-73)
Coadded (1yr) - LSC	0.182	(209,78)
Coadded (1yr) - Disk	0.144	(137,50)
Coadded (3yr) - LSC	0.155	(314,-10)
Coadded (3yr) - Disk	0.108	(122,50)
ILC (1yr) - LSC	0.219	(141,77)
ILC (1yr) - Disk	0.222	(144,65)
ILC (3yr) - LSC	0.216	(133,74)
ILC (3yr) - Disk	0.155	(129,61)

TABLE II: Rotated foregrounds with the highest likelihoods, obtained by maximizing P_{Tot} in the cleaned maps. We have normalized the foregrounds by their quadrupoles, which we set to be $C_2^{Fgrd} \approx 60\mu K^2$. In terms of the HFg-LSC model, the parameter $\alpha = 1$. In terms of the HFg-D model, the temperature of the $50^o \times 50^o$ cold spot is $T_{Disk} \approx -130\mu K$.

the quadrupole and the quadrupole-octopole alignment alone are responsible for a factor of 10^2 improvement in P_{38} for the TOH map, and for a factor of ~ 10 improvement in P_{38} for the ILC map.

V. CONCLUSIONS

We have presented circumstantial evidence that an extended foreground near the dipole axis could be distorting the CMB. The subtraction of such a foreground increases the quadrupole, removes the (anomalous) quadrupole-octopole alignment, and dramatically increases the overall likelihood of the CMB maps. Possible physical mechanisms that could account for this foreground are the Sunyaev-Zeldovich effect [25] and the Rees-Sciama effect [27], although it should be noted that both options only work in extreme situations that are probably unrealistic. Another possibility is that a combination of effects is responsible for the foreground. However, if the Sunyaev-Zeldovich effect due to the LSC's gas is indeed responsible for the foreground, it could be directly observed by the Planck satellite [53] within the next few years – see also [51].

We have also shown that the phases of the CMB maps are such that the optimal places for such foregrounds to exist would be around the Local Supercluster, its specular image, or the site of the Local Supercluster rotated 180° around the galactic polar axis. Furthermore, of the two foreground models analyzed here, the non-uniform foreground (HFg-LSC model) seems preferred by the data as it needs a lower overall temperature distortion in order to improve the likelihood of the CMB maps.

[1] D. Spergel *et al.*, arXiv:astro-ph/0603449; G. Hinshaw *et al.*, arXiv: astro-ph/0603451; http://lambda.gsfc.nasa.gov/product/map/current/ .

[2] C. Bennett *et al.*, *Astrophys. J. Suppl.* **148**: 1 (2003); D. Spergel *et al.*, *Astrophys. J. Suppl.* **148**: 175 (2003).

[3] H. K. Eriksen, F. K. Hansen, A. J. Banday, K. M. Gorski and P. B. Lilje, *Astrophys. J.* **605**: 14 (2004); Erratum *ibid.* **609**: 1198 (2004).

[4] A. de Oliveira-Costa, M. Tegmark, M. Zaldarriaga and A. Hamilton, *Phys. Rev.* **D69**: 063516 (2004).

[5] G. Efstathiou, *Mon. Not. Roy. Astron. Soc.* **348**: 885 (2004).

[6] E. Gaztañaga *et al.*, *MNRAS* **346**: 47 (2003).

[7] C. J. Copi, D. Huterer, and G. D. Starkman, *Phys. Rev.* **D70**, 043515 (2004).

[8] D. Schwarz, G. Starkman, D. Huterer and C. Copi, *Phys. Rev. Lett.* **93**: 221301 (2004); C. Copi, D. Huterer, D. Schwarz and G. Starkman, arXiv: astro-ph/0508047.

[9] K. Land and J. Magueijo, *Phys. Rev. Lett.* **95**: 071301 (2005); *Mon. Not. Roy. Astron. Soc.* **362**: 838 (2005).

[10] A. de Oliveira-Costa and M. Tegmark, arXiv: astro-ph/0603369

[11] C. Copi, D. Huterer, D. Schwarz, and G. Starkman, arXiv: astro-ph/0605135

[12] F. Hansen, P. Cabella, D. Marinucci and N. Vittorio, *Astrophys. J.* **607**: L67 (2004).

[13] H. Eriksen, F. Hansen, A. Banday, K. Górski and P. Lilje, *Astrophys. J.* **605**: 14 (2004).

[14] K. Gorski *et al.*, *Astrophys. J.* **464**: L11 (1996); E. Wright *et al*, *Astrophys. J.* **464**: L21 (1996).

[15] J.-P. Uzan, U. Kirchner and G. Ellis, *Mon. Not. R. Astron. Soc.* **344**: L65 (2003).

[16] J.-P. Luminet, J. Weeks, A. Riazuelo, R. Lehoucq and J.-P. Uzan, *Nature* **425**: 593 (2003).

[17] B. Mota, G. Gomero, M. Rebouças and R. Tavakol, *Class. Quant. Grav.* **21**: 3361 (2004).

[18] C. Contaldi, M. Peloso, L. Kofman and A. Linde, *JCAP* **0307**: 002 (2003); J. Cline, P. Crotty and J. Lesgourgues, *JCAP* **0309**: 010 (2003); B. Feng and X. Zhang, *Phys. Lett.* **B570**: 145 (2003); S. Tsujikawa, R. Maartens and R. Brandenberger, *Phys. Lett.* **B574**: 141 (2003); Y.-S. Piao, B. Feng and X. Zhang, *Phys. Rev.* **D69**: 103520 (2004);

[19] J. Martin and C. Ringeval, *Phys. Rev.* **D69**: 083515 (2004); *Phys. Rev.* **D69**: 123703 (2004); *JCAP* **0501**: 007 (2005).

[20] G. Katz and J. Weeks, *Phys. Rev.* **D70**: 063527 (2004). J. Weeks, arXiv: astro-ph/0412231.

[21] M. Tegmark, A. de Oliveira-Costa and A. Hamilton, *Phys. Rev.* **D68**: 123523 (2003).

[22] H. Eriksen et al. *Astrophys. J.* **612**: 633 (2004).

[23] R. C. Helling, P. Schupp and T. Tesileanu, arXiv: astro-ph/0603594.

[24] L. R. Abramo, A. Bernui, I. S. Ferreira, T. Villela and C. A. Wuensche, arXiv: astro-ph/0604346.

[25] L. R. Abramo and L. Sodré Jr., arXiv: astro-ph/0312124.

[26] S. Prunet, J.-P. Uzan, F. Bernardeau and T. Brunier, *Phys. Rev.* **D71**: 083508 (2005).

[27] A. Rakic, S. Rasanen and D. J. Schwarz, arXiv: astro-ph/0601445.

[28] K. T. Inoue and J. Silk, arXiv: astro-ph/0602478.

[29] P. Vielva *et al.*, Astrophys. J. **609**, 22 (2004); M. Cruz, *et al.*, Mon. Not. R. Astron. Soc. **356**, 29 (2005).; M. Cruz *et al.*, arXiv: astro-ph/0603859.

[30] K.M. Górski *et al.*, *Astrophys. J.* **622**: 759 (2005); http://healpix.jpl.nasa.gov/ .

[31] R. Tully, *Astrophys. J.* **257**: 389 (1982); G. Giuricin, C. Marinoni, L. Ceriani and A. Pisani, *Astrophys. J.* **543**: 178 (2000); C. Marinoni, G. Giuricin and A. Pisani, arXiv: astro-ph/0001140; C. Marinoni, G. Giuricin, L. Ceriani, and A. Pisani, in "Cosmic Flows Workshop", ASP Conference Series, Vol. 201, Ed. S. Courteau and J. Willick (2000), arXiv: astro-ph/9909444.

[32] R. Sunyaev and Ya. Zeldovich, *Ap&SS* **7**: 3 (1970); *Comments Astrophys. Space Phys.* **4**: 173 (1972).

[33] J. Carlstrom, G. Holder and E. Reese, *Annu. Rev. Astron. Astrophys.* **40**: 643 (2002); M. Birkinshaw, *Phys. Rept.* **310**: 97 (1999); idem, arXiv: astro-ph/0307177; Y. Rephaeli, *Annu. Rev. Astron. Astrophys.* **33**: 541 (1995).

[34] L. Grego *et al.*, *Astrophys. J.* **552**: 2 (2001); B. Mason, S. Myers and A. Readhead, *Astrophys. J.* **555**: L11 (2001); M. de Petris *et al.*, *Astrophys. J.* **574**: L119 (2002).

[35] R. Cen and J. Ostriker, *Astrophys. J.* **514**: 1 (1999); *ibidem*, **517**: 31 (1999).

[36] A. Kravtsov, A. Klypin and Y. Hoffman, *Astrophys. J.* **571**: 563 (2002).

[37] K. Sembach, arXiv: astro-ph/0311089.

[38] L. Phillips, J. Ostriker and R. Cen, *Astrophys. J.* **554**: L9 (2001).

[39] F. Nicastro *et al.*, *Nature* **433**: 495 (2005).

[40] C. Hogan, *Astrophys. J.* **398**: L77 (1992).

[41] S. Pravdo *et al.*, *Astrophys. J.* **234**: 1 (1979).

[42] S. Molnar and M. Birkinshaw, *Astrophys. J.* **497**:1 (1998).

[43] S. Boughn, *Astrophys. J.* **526**: 14 (1999).

[44] R. Kneissl, R. Egger, G. Hasinger, A. Soltan and J. Trümper, *Astron. Astrophys.* **320**: 685 (1997).

[45] A. Diaferio, A. Nusser, N. Yoshida and R. Sunyaev, *MNRAS* **338**: 433 (2003); A. Diaferio, R. Sunyaev and A. Nusser, *Astrophys. J.* **533**: L71 (2000).

[46] S. Molnar and M. Birkinshaw, *Astrophys. J.* **537**: 542 (2000).

[47] E. Komatsu and U. Seljak, *MNRAS* **336**: 1256 (2002); *MNRAS* **327**: 1353 (2001).

[48] S. Sadeh and Y. Rephaeli, *New Astron.* **9**: 159 (2004).

[49] E. Shaya, P. J. Peebles and R. Tully, *Astrophys. J.* **454**: 15 (1995).

[50] D. Fixsen, G. Hinshaw, C. Bennett and J. Mather, *Astrophys. J.* **486**: 623 (1997); D. Fixsen, *Astrophys. J.* **594**: L67 (2003).

[51] K. Dolag, F. Hansen, M. Roncarelli and L. Moscardini, *Mon. Not. Roy. Astron. Soc.* **363**: 29 (2005).

[52] S. Ettori and A. Fabian, *MNRAS* **305**: 834 (1999).

[53] http://astro.estec.esa.nl/SA-general/Projects/Planck/